Journal of Materials Research and Technology 40 (2026) 1166–1178

Contents lists available at ScienceDirect

Journal of Materials Research and Technology

journal homepage: www.elsevier.com/locate/jmrt

Investigation of surface morphology and properties of aluminium alloy oxide composite coating incorporated with carbon nanotubes and graphene nanoplatelets

Nik Hafizuddin Effandi Nazila [a], Hasnol Hadi Zakaria [b], Sin Tee Tan [a], Md Shuhazlly Mamat [a], Shahira Liza [b], Mohd Hafis Sulaiman [c], Kar Fei Chan [a,d], Masaki Tanemura [e], Yazid Yaakob [a,f,*]

[a] Department of Physics, Faculty of Science, Universiti Putra Malaysia, UPM, 43400, Serdang, Selangor, Malaysia
[b] Tribology and Precision Machining iKohza (TriPreM), Malaysia Japan International Institute of Technology, Universiti Teknologi Malaysia, Jalan Sultan Yahya Petra, 54100, Kuala Lumpur, Malaysia
[c] Department of Mechanical and Manufacturing Engineering, Faculty of Engineering, Universiti Putra Malaysia, 43400, Serdang, Selangor, Malaysia
[d] Department of Materials, Manufacturing and Industrial Engineering, Faculty of Mechanical Engineering, Universiti Teknologi Malaysia, Skudai, Johor, 81310, Malaysia
[e] Department of Physical Science and Engineering, Nagoya Institute of Technology, Gokiso-cho, Showa-ku, Nagoya, 466-8555, Japan
[f] Halal Products Research Institute, Universiti Putra Malaysia, UPM, 43400, Serdang, Selangor, Malaysia

ARTICLE INFO

Keywords:
Anodic aluminium oxide
Carbon nanotubes
Graphene nanoplatelets
Surface properties
Hardness

ABSTRACT

Graphene Nanoplatelets (GNPs) and Carbon Nanotubes (CNTs) offer excellent properties but often suffer agglomeration when used individually. This work investigates hybridizing CNTs and GNPs as reinforcement strategy to improve dispersion and enhance the surface and mechanical properties of Anodic Aluminium Oxide (AAO). Composite coatings were fabricated by incorporating 5g of CNT:GNP mixtures with varying ratios under specific anodizing conditions (60 min in 20 % diluted H_2SO_4). XRD analysis confirmed that AAO and carbon-reinforced AAO composites exhibited orthorhombic and γ-Al_2O_3 phases with no detrimental phase transformations caused by carbon addition. Surface morphology characterization using a 3D Profiler showed that the hybrid 0.5CNT:0.5GNP produced surface roughness of (5.701 μm) and pore dimensions (w: 50.10 μm and d: 60.13 μm) lower than AAO and AAOCNT. SEM-EDX analysis further verified these findings, indicating that CNT-GNP incorporation effectively reduces porosity. The Vicker hardness of 0.5CNT:0.5GNP showed the highest value of 240.3 HV, outperforming AAO (133 HV), AAOCNT (186.2 HV), and AAOGNP (171 HV). The superior performance of the hybrid composite demonstrates that combining CNTs and GNPs effectively mitigates agglomeration and significantly enhances the structural integrity of AAO coatings. These findings provide new insights into carbon-reinforced AAO fabrication and highlight the potential of CNT-GNP hybrids for advanced surface engineering of aluminium alloys.

1. Introduction

Aluminium alloys' advantageous properties, including their strength, corrosion resistance, and especially lightweight nature, make them widely used today in various kinds of industries such as aerospace and transportation [1]. Despite these advantages, aluminium alloys have intrinsic limitations such as low surface hardness, which affects tribological qualities and might undergo plastic deformation under sliding conditions due to poor hardness [2]. Especially in harsh environments, these limitations restrict the material's performance [3]. Recent studies have continued to explore advanced aluminium alloy processing and enhancement methods. For example, wire-based friction stir additive remanufacturing has been used to repair volumetric defects in aluminium alloy components, achieving improved mechanical integrity [4]. Wire-based friction stir welding has also demonstrated equal-strength joining even with assembly gaps, enhancing the adaptability of solid-state joining techniques [5]. Additionally, bonding mechanisms between Cu coatings and aluminium substrates have been further clarified through combined simulations and experiments, offering insight into interfacial strengthening [6].

* Corresponding author. Department of Physics, Faculty of Science, Universiti Putra Malaysia, UPM, 43400, Serdang, Selangor, Malaysia.
E-mail address: yazidakob@upm.edu.my (Y. Yaakob).

https://doi.org/10.1016/j.jmrt.2025.12.239
Received 23 September 2025; Received in revised form 11 December 2025; Accepted 22 December 2025
Available online 23 December 2025

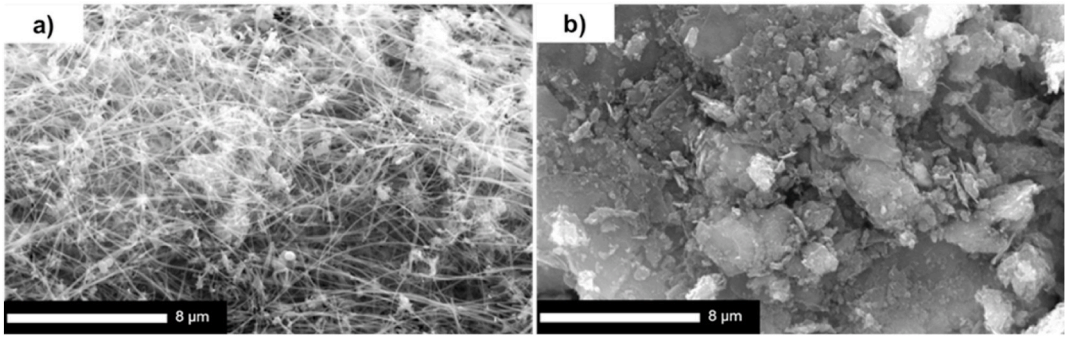

Fig. 1. Surface morphology of a) carbon nanotubes (75.5 nm) and b) graphene nanoplatelets (2600 m^2/g).

Anodizing is one of the most popular and effective surface treatments developed to resolve these issues and improve the functioning and durability of aluminium alloys [7]. AAO contains many small nanopores that can potentially give rise to the formation of cracks. The formation of cracks will cause stress at the surface of AAO which can eventually reduce the overall hardness of the material increasingly [8].

The electrochemical process of anodizing significantly improves the aluminium resistance to corrosion and wear through the formation of a protective oxide coating on its surface [9]. Despite these advantages of anodizing, the process leaves the aluminium with some sort of surface roughness, which lowers its overall strength and tribological properties when challenged by mechanical stresses [10]. Also, high wettability is an expected feature of anodized aluminium oxide coatings, which reduces reinforcement adhesion, resulting in a decline of the material's mechanical properties [11].

The application of reinforcement materials, especially carbon-based reinforcements like CNTs and GNPs, has shown huge potential in enhancing the performance of anodized aluminium. High strength, flexibility, and heat conductivity are only some of these materials' significant mechanical properties [12,13]. CNTs are thought to be extremely promising reinforcing elements for composite materials that are used in metal because of its remarkable mechanical qualities, low density, and wide aspect ratio [14], while GNP has found widespread use as a novel reinforcing filler because of their exceptional qualities, including thermal conductivities, high electrical conductivity, excellent stiffness, and mechanical strength [15]. However, due to their tendency to aggregate when standing alone, adding only the CNTs or GNPs to anodized aluminium alloys presents several issues. These carbon-based reinforcements' ability to improve the anodized aluminium layer is limited by their agglomeration, which causes poor dispersion, uneven reinforcement distribution, and reduced material characteristics [16,17].

Additionally, strong adhesion and successful reinforcement dispersion are difficult to obtain because the high wettability of the coating and the high surface roughness of anodized aluminium oxide. These aspects limit the possibilities of anodizing as a surface treatment for aluminium alloys and cause decreased mechanical performance [18]. Recent studies observed that strong van der Waals interactions promote CNTs agglomeration at high CNTs/GNPs ratios of 4:1 or more, which results in poor dispersion, reduced mechanical performance, and a plateau in electrical conductivity which it is essential to keep the CNTs/GNPs ratio balanced between 1:1 and 2:1 to avoid agglomeration and preserve the synergistic increase of characteristics [19].There also another issue within the composition ratio of CNTs/GNPs is that a high CNTs content causes entanglement and decreased mechanical strength, while a significantly low CNTs content results in GNP-dominated systems with insufficient CNT bridging, fading electrical conductivity [20]. Thus, a major obstacle to producing high-performance anodized aluminium composites is the combination of excessive surface roughness and poor reinforcement dispersion. Since porous surfaces can impair adhesion and durability, the surface morphology of anodized aluminium is a critical factor in defining the mechanical and electrochemical properties of the coating [21]. It is well known that although GNPs tend to fold and stack because of their high aspect ratio, CNTs tend to bundle and agglomerate because of the van der Waals forces. The effects of CNTs and graphene nanoplatelets as the reinforcement particles were investigated in this work. However, excessively high weight percentages of CNTs or GNPs can decrease mechanical strength due to the formation of weak interfacial bonds between the fibers and the matrix [22]. The main objective of this study is to cultivate porous anodic aluminium oxide (AAO) that is then filled with CNTs and GNPs with different ratio. There also are limited research on AAO reinforced CNTs and GNPs via anodization, hence this issue emphasizes the requirement for further improvement of the anodizing process especially to minimize the porosity of the AAO coating to improve its mechanical properties by introducing hybrid reinforcement particles based on carbon materials. The unique aspect of this study is the identification and use of an optimal CNTs/GNPs composition ratio, which improves the hybrid reinforcement particles dispersion and enhances the performance of the AAO coating.

2. Methodology

2.1. Starting material and preparation

Substrate of AA2017-T4 alloy discs with 25 mm diameter and 4 mm thickness, which were purchased from Misumi Malaysia. The primary alloying element inside AA2017-T4 is Copper (Cu) and the chemical composition consists of 91.79 % Al, 5.19 % Cu, and 3.02 % O. Before anodizing, each substrate was ground with silicon carbide abrasive paper (SiC) from 800 grits to 2000 grits to remove surface impurities and essential for accurate measurements, then ultrasonically cleaned with ethanol for 10 min and rinsed with distilled water. This study used Multi-Walled Carbon Nanotubes (≥98 % carbon, density ~2.1 g/mL, Sigma-Aldrich) and Graphene Nanoplatelets (purity ≥98 %, density 2.0–2.5 g/cm^3, Sigma-Aldrich) without further purification as reinforcement particles, as shown in Fig. 1.

2.2. Experimental Setup

This anodizing process utilised a DC power supply. A two-electrode electrochemical cell was used for the anodization process, with a copper plate (99.9 % pure solid copper with 200 mm × 200 mm x 0.5 mm) acting as the cathode and an aluminium alloy as the anode. This study used sulphuric acid (H_2SO_4 (95–98 %), R&M Chemicals), which was diluted to 20 % and to ensure a similar oxide layer fabrication, the electrolyte was initially carried out at room temperature. For 60 min, the anodization process was carried out at a constant 15 V voltage. The aluminium alloy samples were ultrasonically cleaned for 10 min in methanol and washed with distilled water to reduce the surface impurities before anodization.

The reinforcing materials were added by dispersing 5 g/L of

Table 1
Anodizing parameters.

Cathode, Anode	Cu, AA2017
Applied Voltage and Current	15 V, 2 A
Initial temperature	Room temperature
Electrolyte	20 % H_2SO_4
Anodizing time (min)	60
Concentration of Reinforcement Particles (g/L)	5

Table 2
Anodizing Composition Ratio and sample abbreviation.

Sample	Reinforcement Ratio (CNT: GNP)	Label
Anodic aluminium oxide	0: 0	AAO
Anodic aluminium oxide-Carbon nanotube composite	1: 0	AAOCNT
Anodic aluminium oxide-Graphene nanoplatelets composite	0: 1	AAOGNP
Anodic aluminium oxide-carbon nanotube and graphene nanoplatelets composite	0.5: 0.5	0.5CNT:0.5GNP
	0.25: 0.75	0.25CNT:0.75GNP
	0.75: 0.25	0.75CNT:0.25GNP

graphene nanoplatelets (GNPs) and multi-walled carbon nanotubes (CNTs) in the electrolyte using magnetic stirring and ultrasonication to reduce agglomeration. This study examined five distinct CNTs-GNPs compositions: 0:1 (5 g GNPs), 1:0 (5 g CNTs), 0.5: 0.5 (2.5 g CNTs: 2.5 g GNPs), 0.25: 0.75 (1.25 g CNTs: 3.75 g GNPs), and 0.75: 0.25 (3.75g CNTs: 1.25g GNPs). Throughout the anodization process, constant stirring was used to guarantee that the reinforcement particles in the oxide layer were evenly distributed. The parameters for anodizing and the composition ratios with sample abbreviations are concluded in Tables 1 and 2.

The samples were rinsed with distilled water and air-dried at room temperature after anodization. The structural, morphological, and mechanical characterisation of the resultant anodic aluminium oxide (AAO) coatings was then conducted to determine how CNTs-GNPs hybridisation affected the surface characteristics.

2.3. Characterisation

X-ray diffractometer (XRD, PW 3040/60 MPD X'pert Pro Panalytical, Philips, Netherlands) was used to determine the phase composition analysis of AAO and AAO with varying composition ratios in the 2θ range of 20–80°. Then, a 3D optical profiler was used to determine the surface roughness and pore diameters, and the surface topography images were analysed using ZeGage™. The coating's surface morphology and elemental composition were examined using scanning electron microscopy with EDX (SEM-EDX, JEOL JSM IT-100, United States). The Micro Vickers Hardness (HM-G30 Shimadzu Corporation, Japan) was used for measuring the coating's mechanical characteristic of microhardness.

3. Results and discussions

3.1. Voltage and electrolyte temperature to time responses

The electrolyte temperature-time curve and voltage obtained during the anodizing of AA2017 in the electrolyte with and without a 5 g/L variety ratio of reinforcement particles using direct current (DC) are shown in Fig. 2. The anodizing process's voltage and electrolyte temperature are extremely important because they will affect the anodic film's ultimate chemistry, shape, and characteristics [23]. The thickness of the oxide film with broader and larger holes can increase with an increase in the applied voltage [24]. During anodizing, the heat transfer affects the electrolyte temperature. During Joule heating process, which is caused by ionic current passing through the extremely resistant oxide layer of the aluminium substrate, is the primary method of producing heat [25]. Also, when aluminium dissolved chemically, the electrolyte conductivity raised the temperature, which caused an oxide layer to grow on the surface of AA2017 while causing pore broadening close to the oxide/electrolyte contact due to high electrolyte temperatures. The electrolyte becomes aggressive and accelerates the oxide dissolution process at higher temperatures [26]. Based on Fig. 2, during the anodizing process, the electrolyte temperature increases linearly while the voltage value drops for all composite oxide layers. It can be seen that the anodizing process voltages at 10, 30, and 60 min are 10, 8, and 6 V, respectively, after the fabrication process. Since the current density is

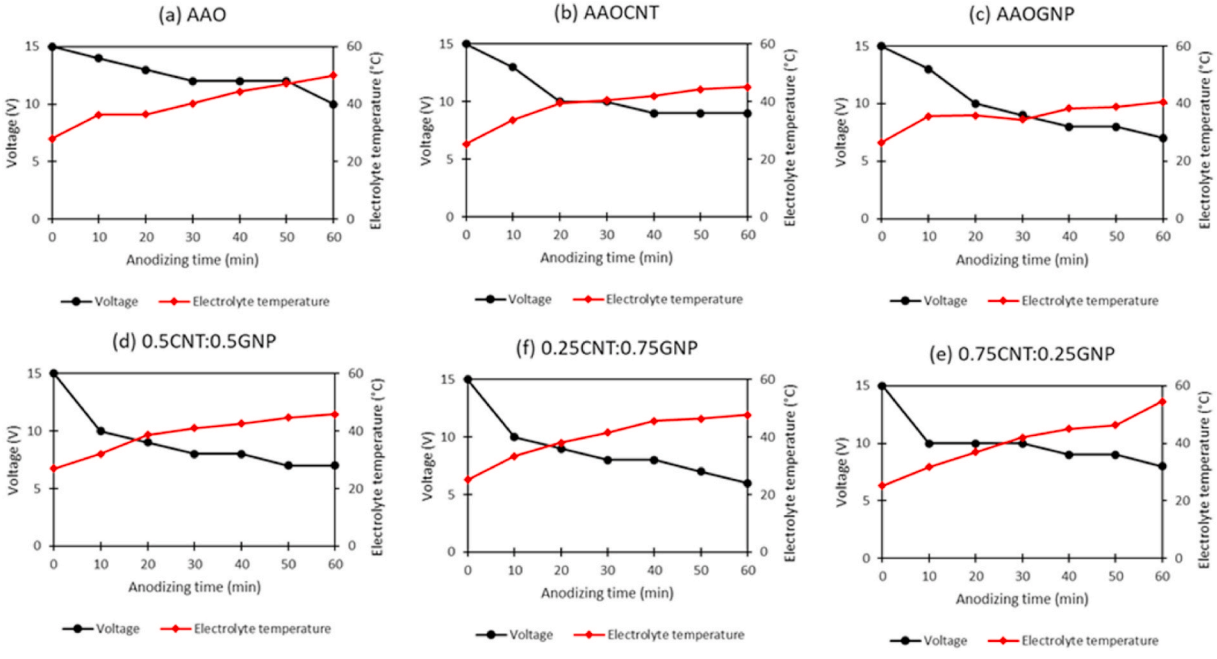

Fig. 2. The voltage and electrolyte temperature vs. anodizing time curve.

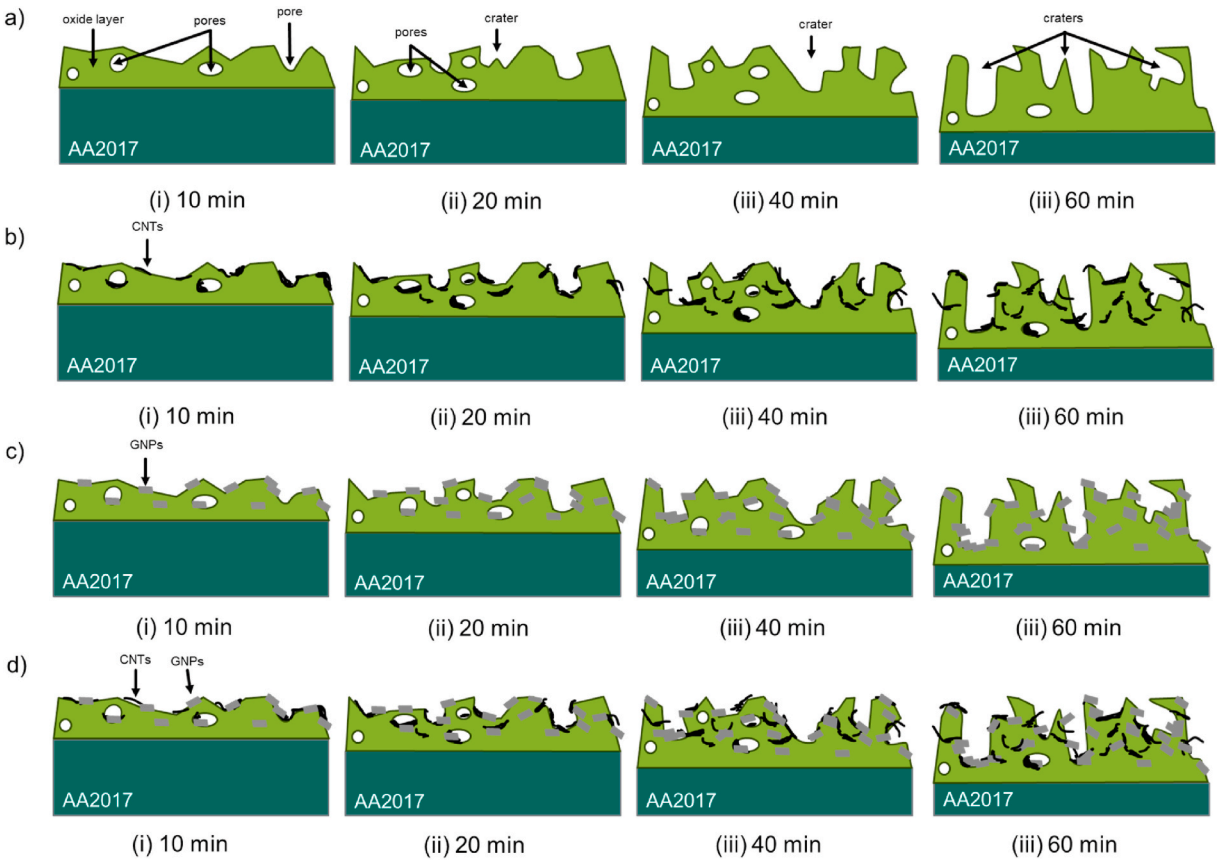

Fig. 3. Growth mechanism of: (a) AAO, (b) AAOCNT, (c) AAOGNP, and (d) CNT:GNP at different time.

maintained at 15 A/dm^2 throughout the anodizing process, there are no noticeable differences in the potential drops for either of the composite oxide films. After 10 min or more, the bubbles produced on the top surface of the electrolyte near the anode and cathode were getting progressively smaller over time. It showed that the aluminium alloy surface had been covered with diluted sulphuric acid and started with oxide formation, demonstrating growth in the coating's thickness [27]. The addition of CNTs and GNPs further influences the electrical behaviour of the electrolyte. Due to their high intrinsic electrical conductivity and aspect ratio, CNTs and GNPs create local conductive pathways within the electrolyte and oxide pores [28]. These pathways facilitate increased ionic mobility and more uniform current distribution across the anode surface. As a result, the electrochemical kinetics are modified, leading to enhanced charge transfer and localized Joule heating [29]. This explains why the electrolyte temperature rises slightly faster, and the voltage declines more gradually for composite coatings compared to pure AAO. The specific ratio of CNTs to GNPs affects the connectivity of these conductive networks, where higher CNT content promotes longitudinal current pathways, while GNPs with larger lateral dimensions enhance planar conduction and pore coverage. Consequently, the macroscopic voltage drop and temperature increase during anodization can be directly linked to the presence, type, and ratio of these conductive nanofillers [30].

The growth mechanism, as illustrated in Fig. 3 correlates with the voltage-time profile in Fig. 2, can be categorized into three stages based on Fig. 2: (i) an initial linear voltage decrease, corresponding to the formation of a barrier layer on the Al surface; (ii) a slight voltage decrease, indicating the development of a composite oxide film through the selective dissolution of barrier oxide into acidic solution; and (iii) a steady-state phase, representing continuous AAO growth [31]. In general, the mechanism can be explained by the chemical reaction that follows: The creation of a barrier layer occurs in stage (i) when Al^{3+} ions move across the metal/oxide interface from the AA2017 surface to form a thin barrier layer [Equation (1)]. Together, during the anodizing or hydrolysis process, the aqueous electrolyte dissociates and produces O^{2-} ions, which migrate to the Al surface.

$$\begin{aligned} Al &\rightarrow Al^{3+} + 3e^- \\ 2H_2O &\rightarrow 2O^{2-} + 4H^+ \end{aligned} \quad (1)$$

It can be seen from Fig. 2, (i) above that the surface of the Al alloy stays comparatively smooth during the early anodization process. Nevertheless, a voltage drop happened as Al^{3+} ions moved and created the compact and dense barrier layer because of its evolution, as shown in Fig. 3. The applied voltage has a direct correlation with the barrier oxide's thickness. In step (ii), O^{2-} ions combine with Al^{3+} ions in the presence of an electric field to form Al_2O_3 [Equation (2)]

$$2Al^{3+} + 3O^{2-} \rightarrow Al_2O_3 \quad (2)$$

Al^{3+} ions provide greater chances for the formation of AAO oxide film growth due to the longer development time. Since ion exchange occurs throughout the anodization process, ion migration occurs simultaneously, including the escape of Al^{3+} and O^{2-} causing the films to develop quickly. As a result, the film develops unstable porosity due to this fast migration. The higher voltage will cause craters to form between adjacent pores. Due to this unstable construction, the voltage was slightly reduced or reached its local maximum as a result of a tiny increase in resistance. There is a correlation between this observation with earlier research [31,32]. Due to chemical anodic dissolution in the formation of dense oxide coatings, it was also noted that the temperature for AAO increased during the anodizing process. Fig. 2 shows that the voltage was nearly constant and had reached its steady-state phase during stage (iii).

During stage (iii), the voltage reaches a near-constant steady-state which indicating stable AAO growth. Prolonged anodizing times

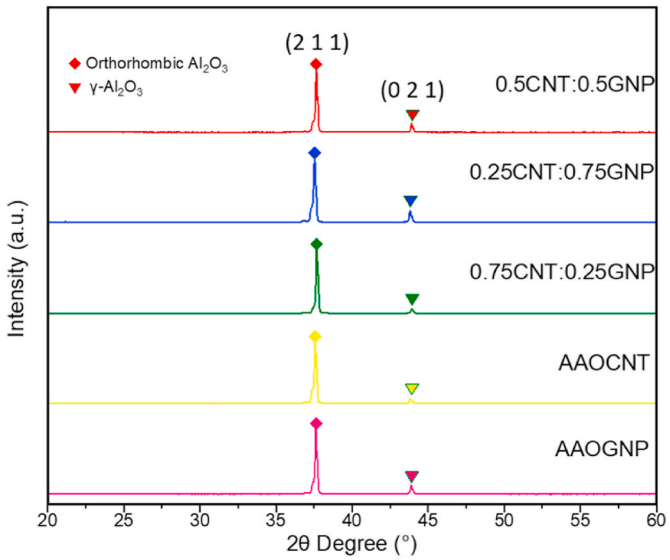

Fig. 4. XRD pattern of anodizing with different composition ratio.

consequently revealed that AAO had increased surface roughness, larger craters on the surface, and more pore formation. Incorporation of CNTs and GNPS into the pores to help with surface porosity, as illustrated in Fig. 3(b–d), which is facilitated by both electrophoresis and self-diffusion [31]. Under the applied electric field, the charged or polarizable CNTs and GNPs migrate toward the Al surface (electrophoresis), while concentration gradients drive self-diffusion within the pores. While stirring process enables the flow of CNTs and GNPs into the pores. CNTs and GNPs tend to migrate from areas of higher concentration to areas of lower concentration during self-diffusion. This self-diffusion can influence the incorporation of CNTs and GNPs into pores and aid in the regularity of their dispersion. Because the anodizing method employed an electric field, it also produced an electrophoresis effect, in which the particles of CNTs and GNPs migrated to the Al surface due to the electric force. Additionally, surface hydroxyl groups and defect sites on Al_2O_3 can interact via van der Waals forces, hydrogen bonding, or π-π interactions with CNTs and GNPs, which stabilise their incorporation and improve dispersion uniformity within the oxide matrix [33]. The combination of these physical and chemical interactions contributes to the formation of a stable composite AAO-CNT/GNP layer with enhanced surface properties, including reduced porosity and improved mechanical strength.

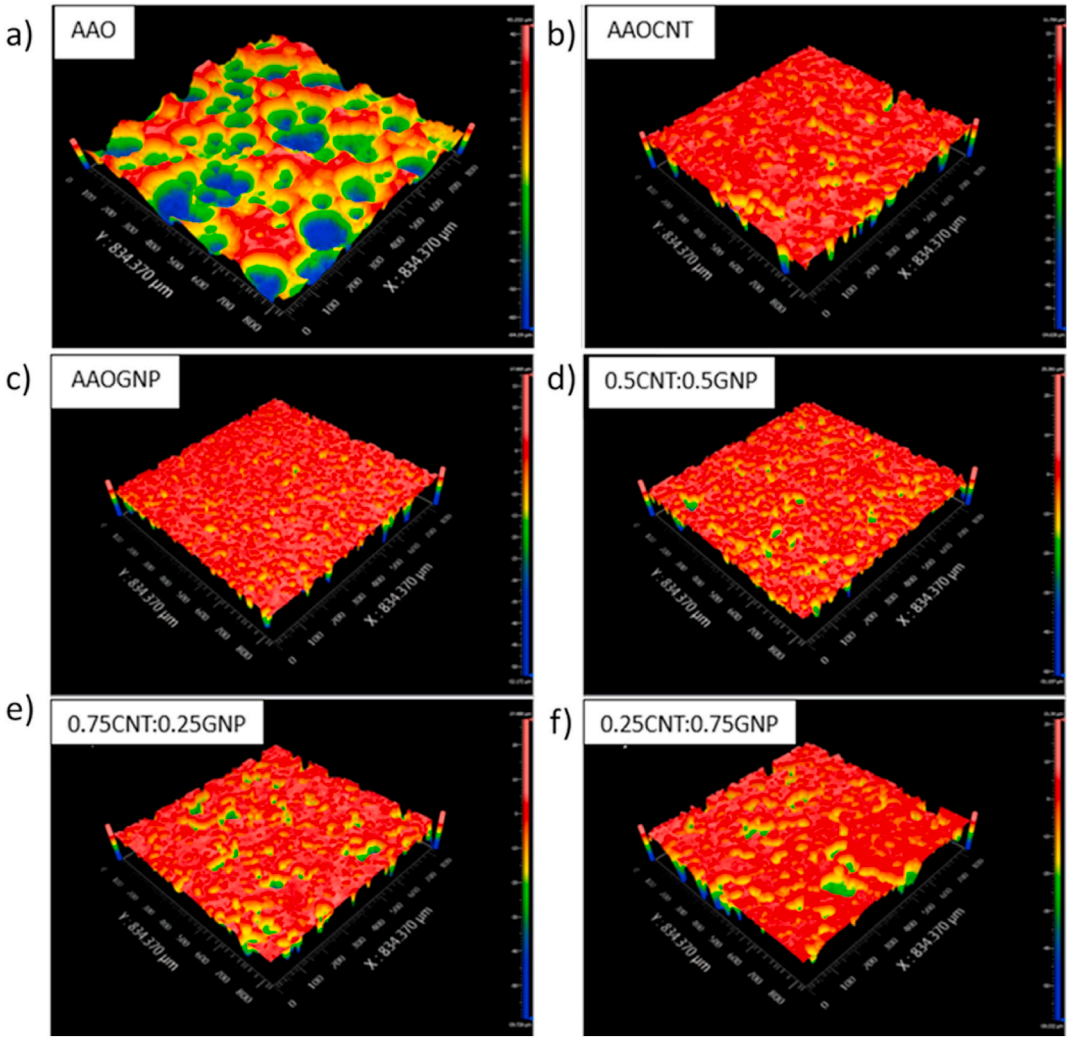

Fig. 5. 3d profilers of a) AAO and AAO with different composition ratio b) AAOCNT, c) AAOGNP, d) 0.5CNT:0.5GNP, e) 0.75CNT:0.25GNP, f) 0.25CNT:0.75GNP.

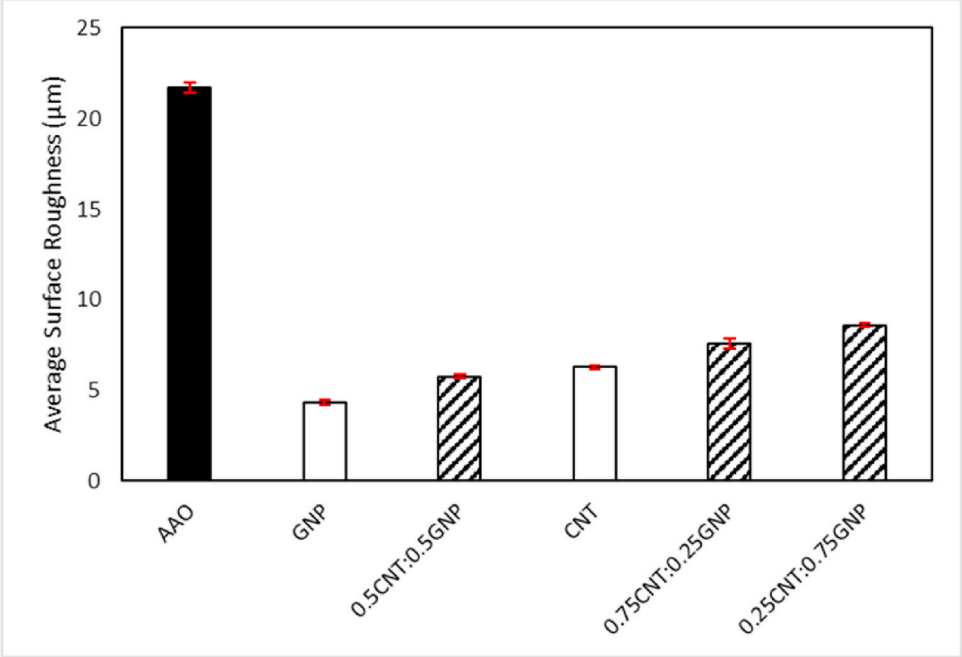

Fig. 6. Average surface roughness of AAO and AAO composites.

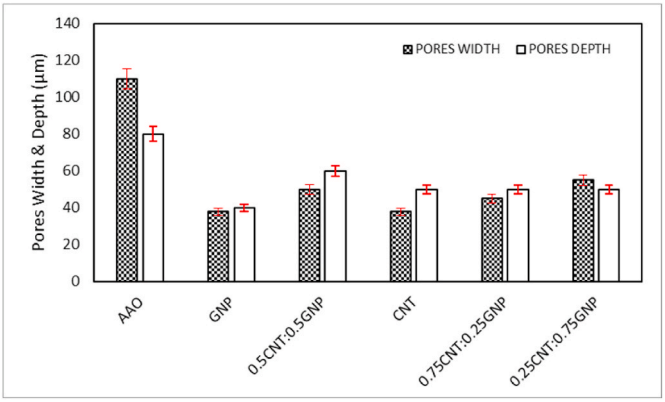

Fig. 7. Average pore dimension of AAO and AAO composites.

3.2. Phase composition analysis

The effect of composition ratio difference on the phase compositions of AAO was determined by XRD analysis. The crystallinity and structural properties of AAO and its composites with different CNTs and GNPs compositions were examined using X-ray diffraction (XRD) analysis. According to the reinforcement compositions, the XRD patterns showed significant differences in peak intensities. The exact positions and intensities of these peaks, which each correlate with specific diffraction angles, provide essential details about the material. The XRD patterns shown in Fig. 4 peaks that correspond to the orthorhombic Al_2O_3 (2 1 1) (JCPDS #98-010- 2358) and Al_2O_3 (0 2 1) (JCPDS #98-001-3124) crystallographic planes, while the XRD data do not show carbon peaks of CNTs or GNPs on the coated surface because of the small quantity 5 g/L of CNTs [32].

3.3. Surface characterization

The 3D profiles of oxide coating surfaces anodized (AAO) and AAO with varying composition of AAOCNT, AAOGNP, 0.5CNT:0.5GNP, 0.75CNT:0.25GNP, and 0.25CNT:0.75GNP are shown in Fig. 5. The topographic images show a series of colour areas categorized in the following order: red, orange, yellow, green, and blue, which represent the crests and troughs of a topographic image [32,34]. The lowest area (trough) is indicated by the blue region, while the highest area (crest) is indicated by the red region. The corresponding average Ra values for these coatings are presented in Fig. 6, while Fig. 7 presents the measured average pore width and depth, demonstrating their correlation with the surface roughness of the composite coating.

Furthermore, in Fig. 5, the AAO displayed numerous large craters and distorted pores, indicative of pronounced pore coarsening during anodization. The incorporation of carbon fillers altered this behaviour: AAOGNP exhibited smoother pores compared to AAOCNT, which can be attributed to the larger lateral dimensions of graphene sheets, helping to physically limit pore expansion and coalescence during oxide growth [35]. The 0.5CNT:0.5GNP hybrid coating resembled AAOCNT in topography, indicating that CNTs dominate the pore morphology at this composition. Conversely, the hybrid coatings with uneven CNT:GNP ratios (0.75CNT:0.25GNP and 0.25CNT:0.75GNP) exhibited slightly increased roughness relative to 0.5CNT:0.5GNP, reflecting enhanced pore coarsening likely caused by uneven filler dispersion and localized disruption of anodic growth kinetics [36].

The distribution and connectivity of CNTs and GNPs indicate a possible percolation threshold within the AAO matrix. At low filler contents, nanomaterials remain mostly isolated, but at higher CNT or GNP fractions, partially connected networks can form within the pores [37]. This percolation can affect surface roughness and pore structure. The slightly higher roughness in 0.75CNT:0.25GNP and 0.25CNT:0.75GNP suggests the onset of such networks, showing that filler type and ratio can modulate interconnected nanofiller pathways and overall surface morphology [38].

Importantly, these variations were reproducible across repeated experiments, indicating that the observed irregular trends are intrinsic to the hybrid system rather than experimental error. The irregularity can be attributed to differences in dispersion stability of CNTs and GNPs within the electrolyte, where GNPs with larger lateral dimensions tend to spread uniformly and reduce surface roughness, while CNTs can form localized agglomerates due to higher surface energy and van der Waals interactions [39]. Additionally, synergistic or antagonistic interactions between CNTs and GNPs at different ratios can influence local anodic

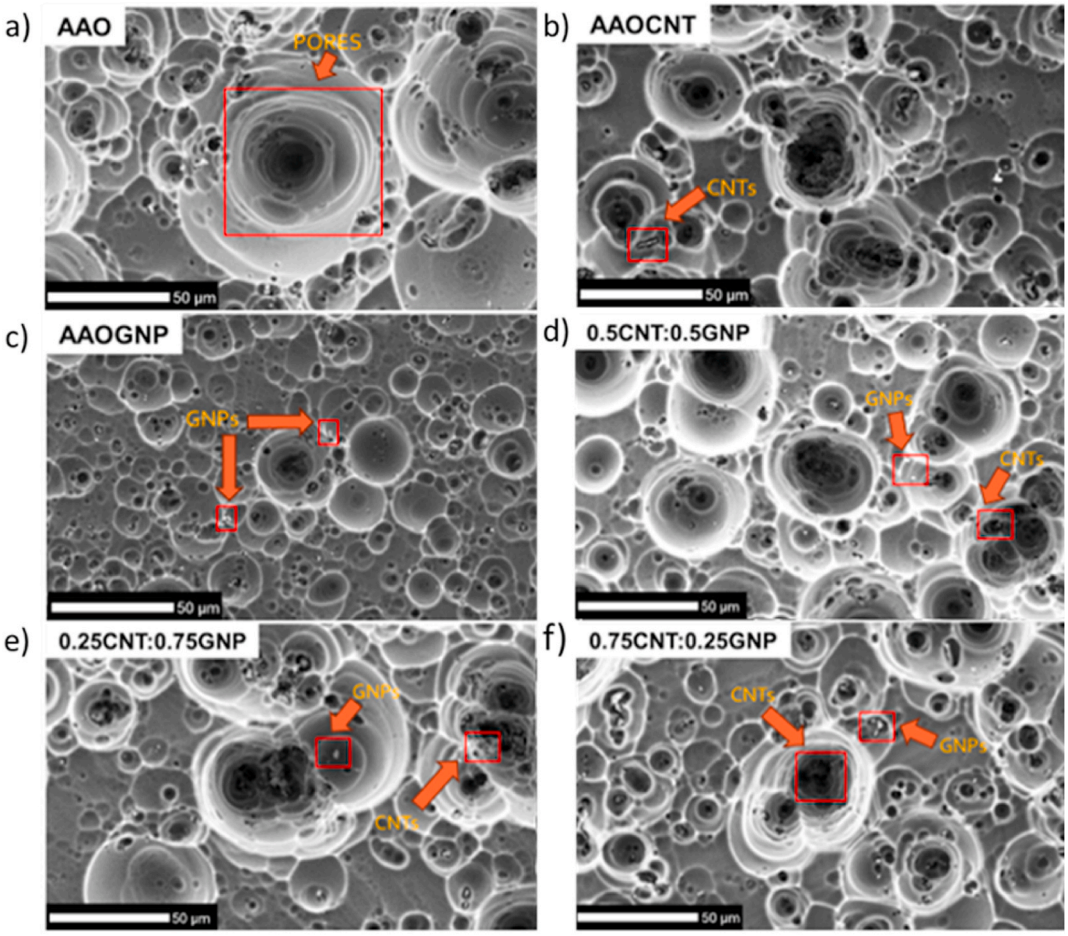

Fig. 8. SEM images focusing on pores and craters of a) AAO and AAO with different composition ratios b) AAOCNT, c) AAOGNP, d) 0.5CNT:0.5GNP, e) 0.75CNT:0.25GNP, f) 0.25CNT:0.75GNP

dissolution and oxide growth, contributing to the composition-dependent variations in Ra and pore dimensions [40].

These results demonstrate that both the type and ratio of carbon additives can effectively tune the surface morphology of AAO-based coatings, providing a strategy to control roughness and pore structure for optimised functional performance.

Fig. 6 shows that the oxide coatings anodized for AAO, AAOCNT, AAOGNP, 0.5CNT:0.5GNP, 0.75CNT:0.25GNP, and 0.25CNT:0.75GNP had average R_a values of 21.704 μm, 6.286 μm, 4.335 μm, 5.763 μm, 7.605 μm, and 8.604 μm, respectively. The addition of reinforcement particles to anodized aluminium oxide (AAO) significantly decreases the surface roughness, with AAOGNP showing the lowest roughness, followed by the CNT0.5:GNP0.5 hybrid composition, AAOCNT, and the other composites. This finding indicates that GNPs have significance in lowering surface roughness because of their excellent dispersion and strong interfacial interactions with the oxide matrix. Previous study on this carbon-based materials also states that the surface roughness decreased by almost 63 % when CNTs were added to the Ni–P matrix, going from 192 nm in the Ni–P coating to 129 nm in the Ni–P-CNT composite [41]. While graphene nanoplatelets have slightly lower surface roughness due to their wide aspect ratio and flat structure, they enable more uniform reinforcement distribution, due to the GNPs ability to spread consistently inside the matrix, which could result in smoother surfaces [42]. In contrast to GNPs, CNTs have a greater surface energy and significant van der Waals forces between nanotubes, which can cause agglomerates. This results in less uniform dispersion and, ultimately, a rougher surface [43]. Based on Fig. 7, AAO without any reinforcement particles have the highest pore dimensions and highest surface roughness, which can also be seen in Fig. 5 images that AAO has enormous craters formed by the merging of the pores upon closer inspection at higher magnification. Also, as shown in Fig. 7, the graphs indicate a considerable reduction in the average width and depth of all AAO with the addition of carbon-based materials into the coating matrix, corresponding towards lower surface roughness as shown in Fig. 5. This confirms that the addition of reinforcement particles reproducibly reduces surface roughness and pore size, consistent with a previous study that both size and quantity of pores can be significantly reduced by the addition of CNTs [44].

From Fig. 8, the SEM images of AAO and its composites with varying reinforcement ratios show significant differences in surface morphology and pore structure. With the same magnification and scale size, AAOGNP exhibit a smaller pore size, which indicates in Fig. 6 that GNP have the lowest surface roughness. Pure AAO, by contrast, exhibits large and irregular pores and surface irregularities with a more open structure, characteristic of anodization without any reinforcement and corresponding to the highest surface roughness. In contrast, AAOGNP shows significantly smaller pores compared to AAOCNT due to the planar structure and high surface area, promotes better dispersion, leading to a more compact oxide layer with uniformly smaller pores [45]. The hybrid composites, such as 0.5CNT:0.5GNP, 0.75CNT:0.25GNP, and 0.25CNT:0.75GNP, exhibit a combination of craters and smaller pores, while CNTs and hybrid compositions produce a rougher surface with crate-like features and slightly larger pores.

As shown in Fig. 9, focusing on the sample of 0.5CNT:0.5GNP, which exhibited the highest microhardness as shown in Fig. 10. The figure shows that CNTs and GNPs are present in the composite coatings as

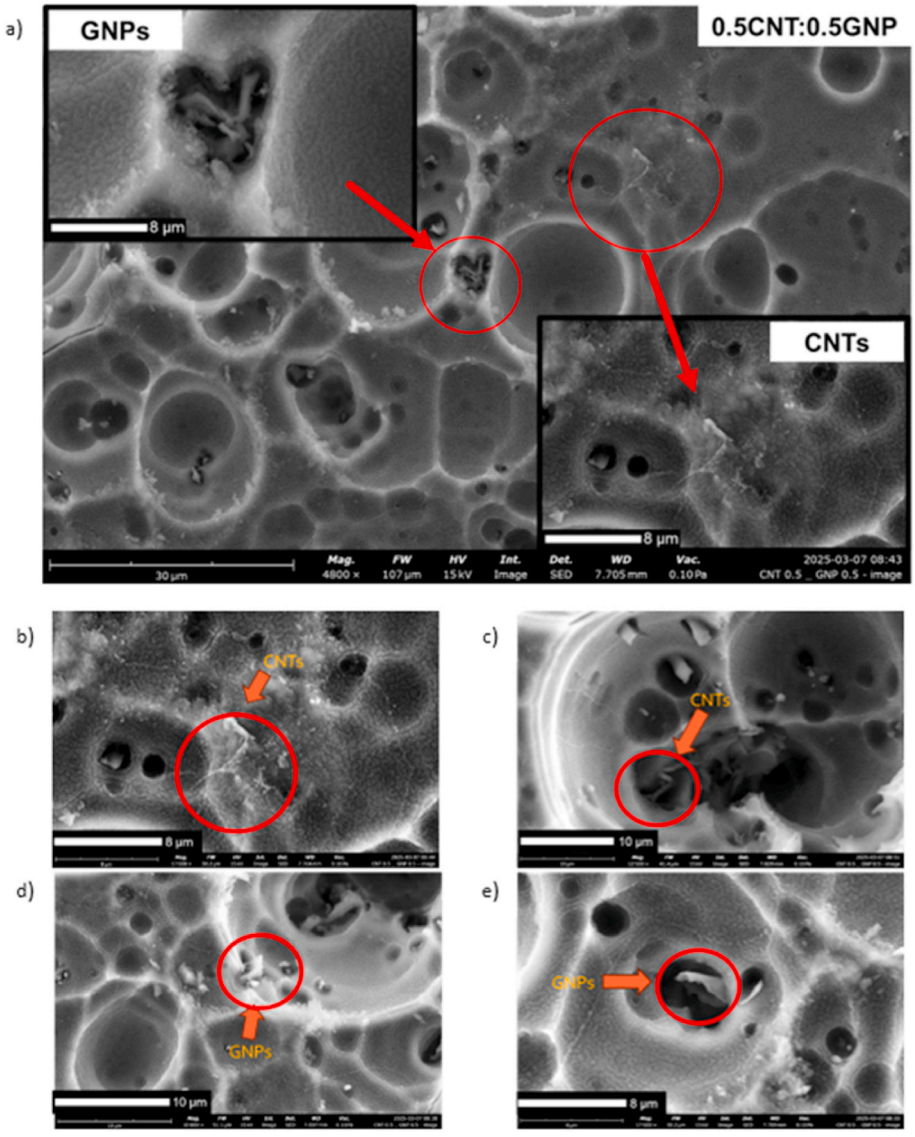

Fig. 9. SEM images of a) 0.5CNT:0.5GNP oxide layer coating surface, b) and c) CNTs on surface and inside pore, d) and e) GNPs on surface and inside pore.

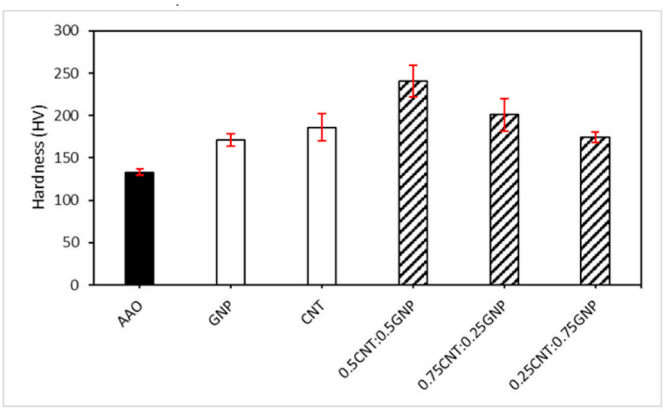

Fig. 10. Average microhardness of AAO and AAO with different composition ratios.

reinforcement particles, and this ratio of reinforcement particles is the optimum value in this research, which can help the particles disperse more evenly within the anodic oxide layer. The reinforcement particles act as barriers and impediments to the crack route, and this dispersion aids in preventing crack initiation and progression because the cracks are resisted by the scattered reinforcing particles, further increasing the material properties to become more resilient [45]. Table 3 shows the carbon weight concentration of GNPs and CNTs. CNTs have hair-like structure, are more easily detected by Energy dispersive X-ray (EDX) because of their surface, whereas GNPs have flake shape, residing inside pores, and are less detectable because electron beam scattering reduces signal resolution when inside pores. The SEM electron beam may scatter, particularly if the pores are narrow or deep which influence the resolution of the EDX signals derived from the inside of the pores may be lowered by this scattering and to getting accurate results may also be more difficult to get due to less effective X-ray collecting from deeper locations caused by the angle at which the electron beam strikes the

Table 3
Chemical compositions of the composite anodic oxide layer coating from Fig. 8.

Spectrum	Weight %			
	C	O	Al	S
GNPs	3.80	43.10	37.60	2.10
CNTs	16.47	46.99	34.14	2.41

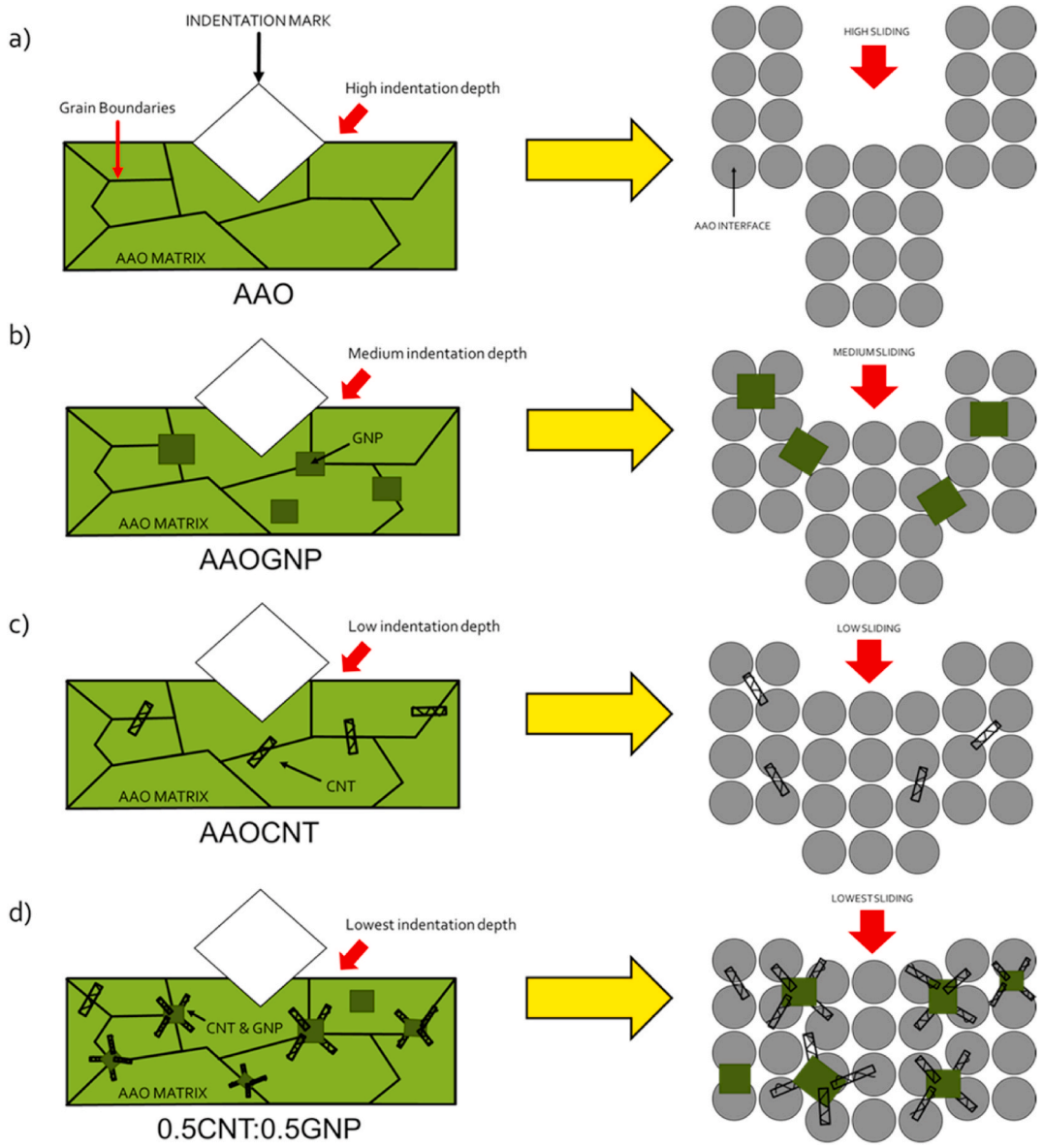

Fig. 11. Illustration of reinforcement particles acting inside the AAO coatings interface, a) AAO, b) AAOCNT, c) AAOGNP, and d) 0.5CNT:0.5GNP.

pores [46].

3.4. Microhardness of composite

The microhardness values of anodized aluminium oxide (AAO) and its composites with varying reinforcement compositions reveal clear trends based on the data shown in Fig. 10. AAO shows the lowest microhardness due to its relatively soft anodized oxide layer [47]. The 0.5CNT:0.5GNP hybrid shows the highest microhardness of 240.3 HV due to compatible behaviours of graphene nanoplatelets (GNPs) and carbon nanotubes (CNTs), which enhance the mechanical characteristics by better dispersion and interlocking within the aluminium oxide matrix. As GNPs' wide surface area helps reduce CNT entanglement, resulting in a more uniform distribution of reinforcements, CNTs' high aspect ratio and flexibility enable them to act as spacers between GNPs, limiting restacking. The CNTs and GNPs interlock to form a strong network structure that efficiently distributes stress, reduces dislocation movement, and raises the hardness of the composite [48]. Besides, AAOGNP exhibits noticeably less microhardness than AAOCNT, indicating that GNPs by themselves are not as successful at increasing hardness as CNTs because of their high aspect ratio and tubular morphology. CNTs form a more interconnected network that effectively prevents dislocation movement and improves load transfer efficiency. This difference can be ascribed to the structural characteristics of the reinforcements. As two-dimensional platelets, GNPs, on the other hand, are more likely to restack and slide inside the anodic aluminium oxide (AAO) matrix when stress is applied, which results in less hardness performance and weaker reinforcement. The CNTs more successfully add to the composite's hardness because of their high tensile strength and stiffness by creating a more cohesive reinforcement network. CNTs lessen structural flaws and significantly increase microhardness [49]. These findings suggest that CNTs offer better reinforcement, particularly in terms of hardness, even though GNPs improve several characteristics. In addition to filler type and composition, the average microhardness of AAO coatings may be influenced by anodization temperature, electrolyte conditions, and oxide layer thickness [50]. Higher temperatures or optimised thermal treatment could enhance hardness by promoting densification of the oxide matrix, while variations in pore morphology and filler dispersion may also modulate the mechanical response of the coatings. Further studies incorporating these parameters could provide

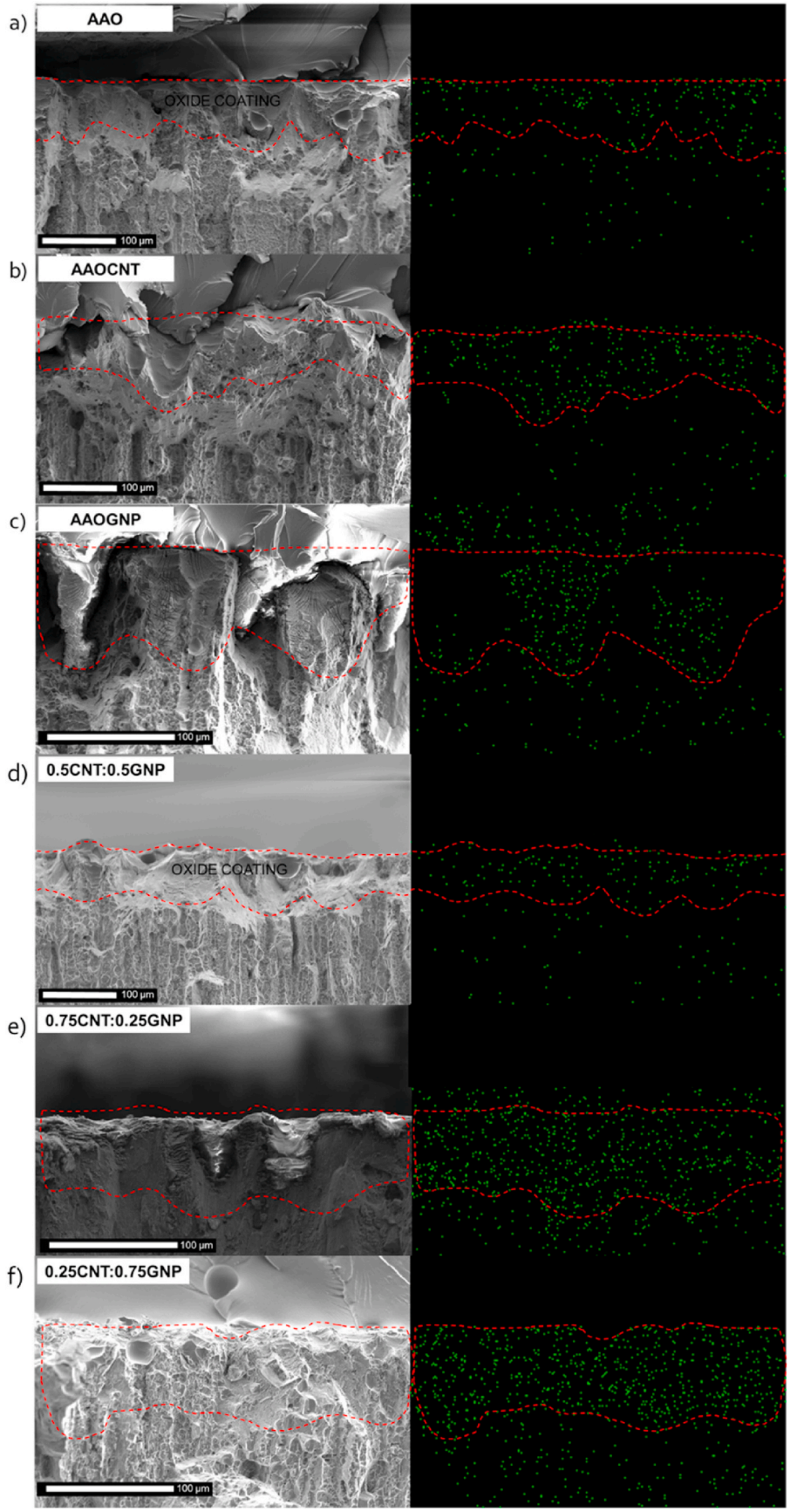

Fig. 12. Cross-sectional SEM images and EDS mapping of oxygen (O) element of AAO with different composite coating ratio.

deeper insight into the microhardness behaviour of AAO-CNT/GNP composites.

As illustrated in Fig. 11, the potential of anodic aluminium oxide (AAO) coatings to withstand interfacial sliding under mechanical stress is a key factor in determining their hardness. Pure AAO interfaces have limited strength and low hardness, which can be seen by the high indentation depth, because the structure can readily slide along grain boundaries and crystallographic planes. After introducing reinforcement particles, specifically GNPs, they can decrease the indentation depth, thus improving hardness by preventing dislocation motion over planar barriers and providing resistance towards interface slip. Furthermore, because of their high surface area and layered structure, which enables them to attach efficiently to the AAO matrix, GNPs aid in mechanical interlocking within the matrix. However, the dispersion of GNPs affects their reinforcing efficiency. The homogeneity and hardness of the coating can be weakened if agglomeration occurs, because GNPs may group together to form clusters that reduce their barrier efficiency and produce stress concentration spots.

Compared to GNPs, CNTs have lower indentation depth and even higher resistance to interface slippage because of their high aspect ratio and tubular structure. CNTs greatly aid in mechanical interlocking with the AAO matrix in addition to blocking dislocation migration in multiple directions. They can physically anchor into the oxide structure thanks to their shape, which improves load transfer and stops local deformation. The hardness enhancement is greater than that of GNPs alone because of their dual function as an interlocking reinforcement and a physical barrier. However, similar to GNPs, CNTs clumping is a significant drawback. The advantages of CNTs reinforcement are reduced due to entangled CNTs bundles, which can also generate structural inhomogeneities and decrease interfacial bonding. For 0.5CNT:0.5GNP, the optimal result is shown; combining GNPs with CNTs in a hybrid reinforcement system tends to enhance both reinforcements' dispersion while utilising their respective advantages, such as the multidirectional pinning of CNTs and the planar blocking of GNPs, thus introducing higher interlocking. This hybrid shows the lowest indentation depth and better dispersion of reinforcement particles, therefore providing the highest resistance to interface slipping. Agglomeration is prevented because of their reciprocal interaction and three-dimensional separation effect; both materials' propensity to agglomerate is lessened when they are present, resulting in a more uniform distribution within the AAO matrix.

A dense, interconnected network that more successfully prevents interface slippage and disperses stress throughout the coating is achieved by this improved dispersion. Because hybrid-reinforced AAO coatings have better reinforcement mechanisms and better structural homogeneity, they attain the maximum hardness. Also, the rough surface of the reinforcement particles, GNPs and CNTs, having irregular shapes, becomes embedded within the matrix material, hence acting as the "interlocking mechanism" of reinforcement particles inside AAO composite coating, while 0.5CNT:0.5GNP shows the highest hardness due to better dispersion of reinforcement particles within the coating matrix. These reinforcement particles create a mechanical "lock" that prevents them from readily detaching, greatly improving the coating's overall strength and adhesion [51]. Overall, CNTs provide more individual reinforcement than GNPs, and when combined with GNPs in a well-dispersed hybrid system, they offer the best way to maximize mechanical performance. Both CNTs and GNPs increase hardness by blocking dislocation motion and interlocking.

The coating thicknesses were determined using cross-sectional SEM supported by oxygen (O) elemental mapping to clearly delineate the oxide layer, as shown in Fig. 12. The average coating thicknesses for AAO and 0.5CNT:0.5GNP were 73.51 ± 12.59 μm and 73.17 ± 6.01 μm, respectively, indicating that the incorporation of carbon-based reinforcements does not significantly influence overall oxide growth. Similar trends were observed for the other reinforced coatings, where AAOCNT (77.41 ± 1.63 μm), AAOGNP (70.37 ± 2.16 μm), 0.25CNT:0.75GNP (70.60 ± 4.39 μm), and 0.75CNT:0.25GNP (71.00 ± 9.47 μm) all exhibited comparable thickness values. These findings suggest that the observed differences in microhardness arise mainly from reinforcement type, composition, and dispersion rather than from variations in coating thickness, thereby minimizing substrate effects during hardness measurements. Minor variations among samples may be attributed to slight changes in local electrolyte temperature or conductivity during anodization [52]. Overall, the results confirm that coating thickness is primarily governed by the anodization parameters, and the addition of CNTs or GNPs does not substantially alter the final oxide layer thickness [53].

4. Conclusions

In conclusion, the aluminium alloy's oxide layer coating on the surface was successfully synthesized with different reinforcement composition ratios. The effect of different ratios of reinforcement particles on the anodizing process was studied. Cross-sectional SEM images revealed that the average coating thicknesses of AAO and the reinforced composites were comparable, ranging from 70.37 ± 2.16 μm to 77.41 ± 1.63 μm. AAO with 0.5CNT:0.5GNP ratio showed, from 3D images, a reduction in pore size and a decrease in surface roughness to 5.763 μm, while exhibiting the highest microhardness of 240.3 HV compared to bare Al alloy and other reinforcement particle ratios. The ratio of 0.5CNT:0.5GNP can be used to enhance the performance of bare Al alloy. This study indicates that 0.5CNT:0.5GNP exhibits promising properties as a potential solution for protective coating uses in automotive and industrial machining applications.

Credit author statement

Nik Hafizuddin Effandi Nazila - Writing – review & editing, Writing – original draft, Visualization, Validation, Methodology, Investigation, Formal analysis, Data curation.

Hasnol Hadi Zakaria - Writing – review & editing, Visualization, Validation, Methodology, Investigation, Formal analysis, Data curation.

Sin Tee Tan - Writing – review & editing, Visualization, Validation, Methodology, Investigation, Formal analysis, Data curation.

Md Shuhazlly Mamat - Writing – review & editing, Validation, Project administration, Formal analysis, Data curation.

Shahira Liza - Writing – review & editing, Visualization, Validation, Resources, Methodology, Investigation, Formal analysis, Data curation.

Mohd Hafis Sulaiman - Writing – review & editing, Validation, Formal analysis, Data curation.

Kar Fei Chan - Writing – review & editing, Validation, Formal analysis, Data curation.

Masaki Tanemura - Writing – review & editing, Validation, Formal analysis, Data curation.

Yazid Yaakob - Writing – review & editing, Writing – original draft, Visualization, Validation, Supervision, Resources, Project administration, Methodology, Investigation, Funding acquisition, Formal analysis, Data curation, Conceptualization.

Declaration of competing interest

The authors declare that they have no known competing financial interests or personal relationships that could have appeared to influence the work reported in this paper.

Acknowledgement

This work was supported by the Ministry of Higher Education, Malaysia. and Universiti Putra Malaysia, Malaysia (MoHE) through the Fundamental Research Grant Scheme (FRGS/1/2022/STG05/UPM/02/3), project number 5540572 and Geran Putra-Inisiatif Putra Siswazah (GP-IPS/2024/9806700), Universiti Putra Malaysia.The authors also

thank Assoc. Prof. Dr. Hidetoshi Miyazaki of Nagoya Institute of Technology and Dr. Mohd Zamri Mohd Yusop of Universiti Teknologi Malaysia for their valuable technical advice.

References

[1] Zhu Z, Hu Z, Seet HL, Liu T, Liao W, Ramamurty U, Ling Nai SM. Recent progress on the additive manufacturing of aluminum alloys and aluminum matrix composites: microstructure, properties, and applications. Int J Mach Tools Manuf 2023;190:104047. https://doi.org/10.1016/j.ijmachtools.2023.104047.

[2] Venkateswarlu K, Varma KPVK, Nutakki UK. Effect of nanoparticle reinforcement and cryogenic treatment on aluminum alloys for enhancement of mechanical and microstructural characteristics-a review. Int J Interact Des Manuf 2024. https://doi.org/10.1007/s12008-024-02106-4.

[3] Callister WD, Rethwisch DG. Materials science and engineering: an introduction. tenth ed. Wiley; 2018.

[4] Huang Y, Xie Y, Chen J, Li J, Zhao Y, Meng X. Wire-based friction stir additive remanufacturing of 2219 aluminum alloy components. Int J Adv Manuf Technol 2025;137:6029–41. https://doi.org/10.1007/s00170-025-15544-5.

[5] Dong W, Meng X, Xie Y, Zhang Z, Tian H, Sun X, Li J, Huang Y. Wire-based friction stir welding enables equal-strength joining of aluminum alloys even with assembling gaps. J Manuf Process 2025;151:426–33. https://doi.org/10.1016/j.jmapro.2025.07.050.

[6] Shao L, Li W, Lu Q, Xue N, Chen Y, Wu Y, Liu C, Liu Y, Sajjad K, Shi Q, Wang C, Lv J, Ye M, Zhou T, Huang J, Zhu L. Bonding mechanism in Cu coating deposited on Al alloy substrate: combining molecular dynamics simulation and experiment. Mater Sci Eng A 2025;942:148703. https://doi.org/10.1016/j.msea.2024.148703.

[7] Raffin F, Echouard J, Volovitch P. Influence of the anodizing time on the microstructure and immersion stability of tartaric-sulfuric acid anodized aluminum alloys. Metals 2023;13:993. https://doi.org/10.3390/met13050993.

[8] Zhang W, Kang K, Wei A, Liu Y, Yang F. Anodizing-induced cracking in the preparation of TiO2 nanotube arrays. Micro Nanostruct 2023;181:207626. https://doi.org/10.1016/j.micrna.2023.207626.

[9] Mehdizade M, Soltanieh M, Eivani AR. Investigation of anodizing time and pulse voltage modes on the corrosion behavior of nanostructured anodic layer in commercial pure aluminum. Surf Coatings Technol 2019;358:741–52. https://doi.org/10.1016/j.surfcoat.2018.08.046.

[10] Abdel-Gawad SA, Osman WM, Fekry AM. Characterization and corrosion behavior of anodized Aluminum alloys for military industries applications in artificial seawater. Surf Interfaces 2019;14:314–23. https://doi.org/10.1016/j.surfin.2018.08.001.

[11] Kim Y, Hwang W, Cho H, Lee J-W. A study on the minute change of the alumina surface structure according to the anodizing conditions for the production of a robust wettability-modified surfaces. Surf Coatings Technol 2022;439:128453. https://doi.org/10.1016/j.surfcoat.2022.128453.

[12] Alasvand Zarasvand K, Golestanian H. Investigating the effects of number and distribution of GNP layers on graphene reinforced polymer properties: physical, numerical and micromechanical methods. Compos Sci Technol 2017;139:117–26. https://doi.org/10.1016/j.compscitech.2016.12.024.

[13] Jung M, Lee Y, Hong S-G, Moon J. Carbon nanotubes (CNTs) in ultra-high performance concrete (UHPC): dispersion, mechanical properties, and electromagnetic interference (EMI) shielding effectiveness (SE). Cem Concr Res 2020;131:106017. https://doi.org/10.1016/j.cemconres.2020.106017.

[14] J M, S S, Prathap H. Electroless nickel plating of arc discharge synthesized carbon nanotubes for metal matrix composites. Appl Surf Sci 2015;324:475–81. https://doi.org/10.1016/j.apsusc.2014.10.150.

[15] Lee C, Wei X, Kysar JW, Hone J. Measurement of the elastic properties and intrinsic strength of monolayer graphene. Science 2008;321:385–8. https://doi.org/10.1126/science.1157996.

[16] Chanteli A, Tserpes KI. Finite element modeling of carbon nanotube agglomerates in polymers. Compos Struct 2015;132:1141–8. https://doi.org/10.1016/j.compstruct.2015.07.033.

[17] Zhou W, Huang Y, Wu Z, Habibi M, Habibi M, Marzouki R. Influence of agglomeration and waviness phenomena on torsional oscillation of MWCNTs-reinforced composite rods. Int J Solids Struct 2025;306:113127. https://doi.org/10.1016/j.ijsolstr.2024.113127.

[18] Buijnsters JG, Zhong R, Tsyntsaru N, Celis J-P. Surface wettability of macroporous anodized aluminum oxide. ACS Appl Mater Interfaces 2013;5:3224–33. https://doi.org/10.1021/am4001425.

[19] Shen X, Wang Z, Wu Y, Liu X, Kim J-K. Effect of functionalization on thermal conductivities of graphene/epoxy composites. Carbon N Y 2016;108:412–22. https://doi.org/10.1016/j.carbon.2016.07.042.

[20] Chen D, Yang J, Kitipornchai S. Nonlinear vibration and postbuckling of functionally graded graphene reinforced porous nanocomposite beams. Compos Sci Technol 2017;142:235–45. https://doi.org/10.1016/j.compscitech.2017.02.008.

[21] Korzekwa J. Modification of the structure and properties of oxide layers on aluminium alloys: a review. Rev Adv Mater Sci 2023;62. https://doi.org/10.1515/rams-2023-0108.

[22] Kumar A, Sharma K, Dixit AR. Carbon nanotube- and graphene-reinforced multiphase polymeric composites: review on their properties and applications. J Mater Sci 2020;55:2682–724. https://doi.org/10.1007/s10853-019-04196-y.

[23] Nielsch K, Choi J, Schwirn K, Wehrspohn RB, Gösele U. Self-ordering regimes of porous alumina: the 10 porosity rule. Nano Lett 2002;2:677–80. https://doi.org/10.1021/nl025537k.

[24] Sullivan JPO, Wood GC. The morphology and mechanism of formation of porous anodic films on aluminium. Proc R Soc London A Math Phys Sci 1970;317:511–43. https://doi.org/10.1098/rspa.1970.0129.

[25] Aerts T, De Graeve I, Terryn H. Study of initiation and development of local burning phenomena during anodizing of aluminium under controlled convection. Electrochim Acta 2008;54:270–9. https://doi.org/10.1016/j.electacta.2008.08.004.

[26] Paz Martínez-Viademonte M, Abrahami ST, Hack T, Burchardt M, Terryn H. A review on anodizing of aerospace aluminum alloys for corrosion protection. Coatings 2020;10:1106. https://doi.org/10.3390/coatings10111106.

[27] Abdel-Gaber AM, Abd-El-Nabey BA, Sidahmed IM, El-Zayady AM, Saadawy M. Kinetics and thermodynamics of aluminium dissolution in 1.0M sulphuric acid containing chloride ions. Mater Chem Phys 2006;98:291–7. https://doi.org/10.1016/j.matchemphys.2005.09.023.

[28] Jiang L, Gao L. Carbon nanotubes–metal nitride composites: a new class of nanocomposites with enhanced electrical properties. J Mater Chem 2005. https://doi.org/10.1039/B409682G.

[29] Zhang B, Yu Y, Liu Y, Huang ZD, He YB, Kim JK. Percolation threshold of graphene nanosheets as conductive additives in $Li_4Ti_5O_{12}$ anodes of Li-ion batteries. Nanoscale 2013. https://doi.org/10.1039/C2NR33099G.

[30] Lin C-C, Lin B-Y. Effects of anodization and heat-treatment on anode electrodes of aluminum electrolytic capacitors. Electrochemistry 2012;80:552–8. https://doi.org/10.5796/ELECTROCHEMISTRY.80.552.

[31] Asadi A, Pourfattah F, Miklós Szilágyi I, Afrand M, Żyła G, Seon Ahn H, Wongwises S, Minh Nguyen H, Arabkoohsar A, Mahian O. Effect of sonication characteristics on stability, thermophysical properties, and heat transfer of nanofluids: a comprehensive review. Ultrason Sonochem 2019;58:104701. https://doi.org/10.1016/j.ultsonch.2019.104701.

[32] Mat Tahir NA, Liza S, Fukuda K, Mohamad S, Hashimi MZF, Yunus MSM, Yaakob Y, Othman IS. Surface and tribological properties of oxide films on aluminium alloy through fly-ash reinforcement. Coatings 2022;12:256. https://doi.org/10.3390/coatings12020256.

[33] Mylvaganam K, Zhang L. Possible chemical bond formation between a carbon nanotube and alumina matrix – a quantum mechanics investigation. Key Eng Mater 2010;443:723–8. https://dx.doi.org/10.4028/www.scientific.net/KEM.443.723.

[34] Mohamad S, Liza S, Yaakob Y. Strengthening of the mechanical and tribological properties of composite oxide film formed on aluminum alloy with the addition of graphite. Surf Coatings Technol 2020;403:126435. https://doi.org/10.1016/j.surfcoat.2020.126435.

[35] Lee J-H, Jang Y, Heo K, Lee J-M, Choi SH, Joo W-J, Hwang S, Whang D. Large-scale fabrication of 2-D nanoporous graphene using a thin anodic aluminum oxide etching mask. J Nanosci Nanotechnol 2013;13:1–8. https://doi.org/10.1166/JNN.2013.7876.

[36] Ciambelli P, Arurault L, Sarno M, Fontorbes S, Leone C, Datas L, Sannino D, Lenormand P, Le Blond Du Plouy S. Controlled growth of CNT in mesoporous AAO through optimized conditions for membrane preparation and CVD operation. Nanotechnology 2011;22:265613. https://doi.org/10.1088/0957-4484/22/26/265613.

[37] Li J, Ma P-C, Chow WS, To CK, Tang BZ, Kim JK. Correlations between percolation threshold, dispersion state, and aspect ratio of carbon nanotubes. Adv Funct Mater 2007;17:3207–15. https://doi.org/10.1002/adfm.200700065.

[38] Shehzad K, Ahmad MN, Hussain T, Mumtaz MW, Shah AT, Mujahid A, Wang C, Ellingsen J, Dang Z-M. Influence of carbon nanotube dimensions on the percolation characteristics of carbon nanotube/polymer composites. J Appl Phys 2014;116:134308. https://doi.org/10.1063/1.4892156.

[39] Zhang M, Alvarez NT, Zhao D, Zhang L, Haase MR, Malik R, Katuscak C, Wang T, Shanov V. A corrugated graphene–carbon nanotube composite as electrode material. Adv Mater Res 2014. https://doi.org/10.1142/S1793984414410190.

[40] Chung C-K, Liao MW, Chang H-C, Chang W-H, Liu TY. On characteristics of pore size distribution in hybrid pulse anodized high-aspect-ratio aluminum oxide with Taguchi method. Microsyst Technol 2013. https://doi.org/10.1007/S00542-012-1633-7.

[41] A S, H S, S A, R B, Parfenov EV, Mukaeva VR, R N. The effect of graphite particle size on the corrosion and wear behaviour of the PEO-EPD coating fabricated on commercially pure zirconium. Surf Coatings Technol 2019;363:301–13. https://doi.org/10.1016/j.surfcoat.2019.02.033.

[42] Yang L, Zhao Q, Hou Y, Hong L, Ji H, Xu L, Zhu K, Shen M, Huang H, He H, Qiu J. Flexible polyvinylidene fluoride based nanocomposites with high and stable piezoelectric performance over a wide temperature range utilizing the strong multi-interface effect. Compos Sci Technol 2019;174:33–41. https://doi.org/10.1016/j.compscitech.2019.02.014.

[43] Lee KM, Ko YG, Shin DH. Incorporation of multi-walled carbon nanotubes into the oxide layer on a 7075 Al alloy coated by plasma electrolytic oxidation: coating structure and corrosion properties. Curr Appl Phys 2011;11:S55–9. https://doi.org/10.1016/j.cap.2011.07.009.

[44] Baig Z, Mamat O, Mustapha M. Recent progress on the dispersion and the strengthening effect of carbon nanotubes and graphene-reinforced metal nanocomposites: a review. Crit Rev Solid State Mater Sci 2018;43:1–46. https://doi.org/10.1080/10408436.2016.1243089.

[45] Musil J. Hard nanocomposite coatings: thermal stability, oxidation resistance and toughness. Surf Coatings Technol 2012;207:50–65. https://doi.org/10.1016/j.surfcoat.2012.05.073.

[46] Goldstein JI, Newbury DE, Michael JR, Ritchie NWM, Scott JHJ, Joy DC. Scanning electron microscopy and X-Ray microanalysis. New York, NY: Springer New York; 2018. https://doi.org/10.1007/978-1-4939-6676-9.

[47] Geim AK, Novoselov KS. The rise of graphene. Nat Mater 2007;6:183–91. https://doi.org/10.1038/nmat1849.
[48] Mujeeb Rahman P, Abdul Mujeeb VM, Muraleedharan K, Thomas SK. Chitosan/nano ZnO composite films: enhanced mechanical, antimicrobial and dielectric properties. Arab J Chem 2018;11:120–7. https://doi.org/10.1016/j.arabjc.2016.09.008.
[49] Herzallah H, Elsayd A, Shash A, Adly M. Effect of carbon nanotubes (CNTs) and silicon carbide (SiC) on mechanical properties of pure Al manufactured by powder metallurgy. J Mater Res Technol 2020;9:1948–54. https://doi.org/10.1016/j.jmrt.2019.12.027.
[50] Liu XZ, Yang JH, Wang G, Song LL, Zhuang GS. Effect of preparation conditions on the performance of anodic aluminum oxide films. Appl Mech Mater 2012;164:223–7. https://dx.doi.org/10.4028/www.scientific.net/AMM.164.223.
[51] Pramanik A, Basak AK, Dong Y, Sarker PK, Uddin MS, Littlefair G, Dixit AR, Chattopadhyaya S. Joining of carbon fibre reinforced polymer (CFRP) composites and aluminium alloys – a review. Compos Part A Appl Sci Manuf 2017;101:1–29. https://doi.org/10.1016/j.compositesa.2017.06.007.
[52] Mohammadi I, Afshar A. Modification of nanostructured anodized aluminum coatings by pulse current mode. Surf Coatings Technol 2015;276:1–8. https://doi.org/10.1016/j.surfcoat.2015.08.004.
[53] Yürektürk Y, Muhaffel F, Baydogan M. Characterization of micro arc oxidized 6082 aluminum alloy in an electrolyte containing carbon nanotubes. Surf Coatings Technol 2015;268:38–45. https://doi.org/10.1016/j.surfcoat.2014.12.058.